A Multiresolution Strategy for Detecting Gravitational Waves Generated by Binary Coalescences

J.M. Innocent and B. Torrésani
CPT, CNRS-Luminy, Case 907, 13288 Marseille Cedex 09, France
(September 16, 1996)

We describe a new strategy for the detection of gravitational waves generated by coalescing binaries. The method is based on the use of a modified version of continuous wavelet transform, which is particularly well adapted to the problem. It is shown that the performances of the algorithm approaches those of conventional matched filter methods, with smaller computational cost. We present numerical results, performed on coalescing binaries signals buried in a stationary noise simulating various detector noises.

I. INTRODUCTION

The past few years have seen a increasing interest in the gravitational wave detection problems. Several experiments have started up in the early 90's, among which the LIGO [1], GEO [14] and VIRGO [8] projects, based on laser interferometric detectors. These projects are expected to be operational by the end of the century. Among the potential sources for gravitational waves, one of the most promising seems to be the coalescing binary systems of black holes or neutron stars. Such systems are expected to produce "clean" signals, for which reliable models are available.

Several approaches for detecting the corresponding signals have been investigated, among which Wiener (matched) filtering methods (see [4] for a review) or resampling methods [36,42]. It is the purpose of this paper to develop an alternative approach, which we believe well adapted to the very nature of the problem.

In the particular case of binary star coalescence detection, the detection problem may be formulated as follows (see for example [16,40] for a review). The signal takes the form

$$f(x) = f_\theta(x - x_0) + n(x) \tag{1}$$

where $f_\theta(x)$ is the reference signal (given in good approximation by various post-Newtonian theories [5]), depending on a set of parameters to be estimated, represented generically by θ, x_0 is the date of coalescence (to be estimated as well) and $n(x)$ is the experimental detector noise, generally modeled as a stationary process whose spectral density is provided by experimentalists.

The traditional answer to the above mentioned detection problem is provided by matched filter techniques. This approach was suggested in the context of binary coalescence detection in [39]. Assuming for the sake of the argument that the parameters θ of the signal are known, a filter is built up from the expected signal and the expected noise as

$$\hat{F}_\theta(k) = \frac{\overline{\hat{f}_\theta(k)}}{\mathcal{E}(k)} \ ,$$

with $\mathcal{E}(k)$ the spectral density of the noise. Now since the parameters are *not* known, it is necessary to construct such a filter (generally called a *template*) for sufficiently many choices of the parameters. However, as may be seen for example in [4], the required number of templates may become very large, maybe too large for practical purpose. From this remark it makes sense to search for alternative methods, which might be sub-optimal (since the matched filter is known to optimize the output signal to noise ratio in the category of linear filters), but more robust and efficient from a computational point of view. This paper describes an alternative approach based on the continuous wavelet transform. Our approach essentially uses the particular form of gravity wave signal emitted by coalescing binaries, and more particularly the fact that it is a *locally monochromatic signal*, thus characterized by a limited number of wavelet coefficients, essentially located on a line in the time-scale plane (the so-called *ridge* of the wavelet transform). We show how such a localization may be exploited within an efficient algorithm, compatible with possible real time implementation.

The wavelet transform was proposed by various authors as a candidate for developing binary coalescence detection schemes [29,31,42]. However to our knowledge its potential has not been fully exploited so far. In addition, wavelet techniques possess other advantages which definitely make them serious candidates not only for detection, but for data compression [44] and even data acquisition as well. We shall not elaborate on these points, and focus from now on on the detection problem.

The paper is organized as follows. After recalling the popular signal models based on post-Newtonian approximations and briefly describing a simple detector noise model in Section II, we describe the version of the continuous wavelet transform we shall be using, and elaborate on its main characteristics which are of interest to us in Section III. Then we describe the algorithm in Section IV and present the results of numerical simulations in Section V. Finally, Section VI is devoted to our conclusions and some prospective remarks.

II. MODELS FOR SIGNALS GENERATED BY BINARY COALESCENCES

We review in this section the models which we shall use for the signals generated by binary coalescences and the detector noise. Let us recall that the signal which will be measured at the detector is a strain, hereafter denoted by $h(x)$, which is the superposition of a gravity wave signal (depending on several physical parameters, among which the masses of the coalescing stars, and the distance of the event), and an additive detector noise.

A. Signal Models

Let us assume that we are given a binary system consisting of two stars of masses m_1 and m_2 respectively, at distance R. Let x_0 be the coalescence date, and let us denote by $M = m_1 + m_2$ the total mass and by $\mu = m_1 m_2/M$ the reduced mass. Following the conventional use, we introduce the so-called *chirp mass*

$$\mathcal{M} = \left(M^2\mu^3\right)^{1/5} ,$$

which governs the shape of the gravity wave. In the Newtonian approximation, the expected reference signal is given by

$$\begin{aligned} h(x) &= \epsilon A\, h_F(x_0 - x) \\ &= \epsilon A (x_0 - x)^\alpha \Theta(x_0 - x) \\ &\quad \cos\left(\Phi - \tfrac{2\pi}{\beta+1} F (x_0 - x)^{\beta+1}\right) , \end{aligned} \tag{2}$$

where $\Theta(x)$ is the Heaviside step function, and

$$\alpha = -\frac{1}{4} , \quad \beta = -\frac{3}{8} . \tag{3}$$

Here, the constants A and F (or more precisely their numerical values) may be interpreted as the signal's local amplitude and frequency one second before coalescence, and Φ is a global phase. The constant ϵ accounts for the polarization of the wave with respect to the detector's orientation. ϵ is always positive and smaller than unity, and is generally modeled as a random variable (see [20] for a detailed analysis). In the sequel, we shall set $\epsilon = 1$ (i.e. assume an optimal orientation) for the sake of simplicity.

The function $h_F(x)$ in (2) will be the central object of this paper.

A and F are related to physical parameters as follows.

$$F = C_F \mathcal{M}^{-5/8} , \tag{4}$$

where the chirp mass $\mathcal{M}$ is expressed in *solar masses*, and the numerical constant C_F is approximately equal to $C_F \approx 151.037$.

$$A = C_A \frac{1}{R} \mathcal{M}^{5/4} , \tag{5}$$

where $\mathcal{M}$ is expressed in *solar masses*, the distance R is expressed in Mpc, and the numerical constant C_A is approximately equal to $C_A \approx 3.367\ 10^{-21}$.

As an example, we display in Figure 1 the signal corresponding to a pair of neutron stars of 1.4 solar masses each, coalescing at a distance $R = 100 Mpc$. Only the last second of signal before coalescence (coalescence date: $x_0 = 61$ sec; sampling frequency: $\nu_s = 1000$ Hz) is displayed.

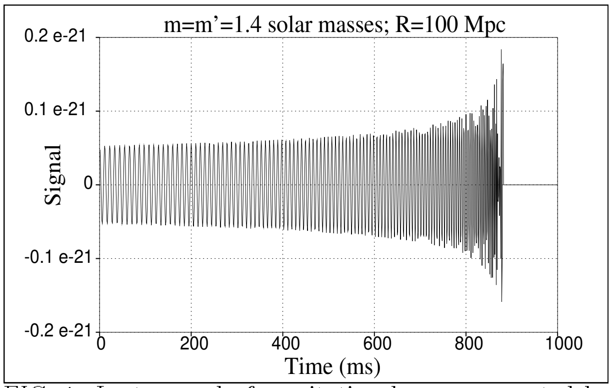

FIG. 1. Last second of gravitational wave generated by a coalescing system of masses $m_1 = m_2 = 1.4 M_\odot$, at a distance $R = 100 Mpc$.

The signal is then an amplitude and frequency modulated one, which means that a local amplitude and a local frequency may be associated with it (we shall reserve the words *instantaneous amplitude* and *instantaneous frequency* for the quantities which may be defined rigorously via the analytic signal, and then term *local* amplitudes and frequencies the quantities which appear in Eq. (2)). The local amplitude and frequency then read

$$A(x) = A(x_0 - x)^\alpha . \tag{6}$$

$$\nu(x) = F(x_0 - x)^\beta . \tag{7}$$

Remarks:

- Notice that according to (2) both the local amplitude and the local frequency diverge as x goes to the coalescence date x_0. However, this problem should not be taken too seriously for the following two reasons. First, Eq (2) is a Newtonian approximation, which is certainly not valid anymore for times close to the coalescence date. Second, the response of the interferometer has to be taken into account, which will force to zero the contribution of very high frequencies.

- Notice also that the signal is in practice buried in a detector noise, whose spectral density diverges as the frequency goes to zero (see Figure 2 and subsection II B below). Therefore, the signal in (2) will presumably be filtered so as to prewhiten the detector noise, in order to reduce quantization noise. The effect of such a prewhitening will in particular be to force to zero both very high and very low frequencies.

More generally, in restricted post-Newtonian approximations (see e.g. [5]), the expected signal may be written in the form

$$h(x) = A\nu(x)^{2/3}\cos\varphi(x) \ , \tag{8}$$

where $\nu(x) = \varphi'(x)$ is the local frequency, and the time-dependent phase $\varphi(x)$ is the sum of several post-Newtonian terms

$$\varphi(x) = \varphi_0(x) + \varphi_1(x) + \varphi_{1.5}(x) + \varphi_2(x) + \dots \ . \tag{9}$$

The correspondence between local frequency and time is given by

$$\begin{aligned} x \ = \ 1+&\tau_0\left[1-\left(\tfrac{\nu(x)}{F}\right)^{-8/3}\right]+\tau_1\left[1-\left(\tfrac{\nu(x)}{F}\right)^{-2}\right] \\ &+\tau_{1.5}\left[1-\left(\tfrac{\nu(x)}{F}\right)^{-5/3}\right]+\dots, \end{aligned} \tag{10}$$

which provides an expression for the *group delay*, i.e. the time of appearance of a given frequency:

$$\begin{aligned} x \ = \ \tau(\nu) = 1+&\tau_0\left[1-\left(\tfrac{\nu}{F}\right)^{-8/3}\right]+\tau_1\left[1-\left(\tfrac{\nu}{F}\right)^{-2}\right] \\ &+\tau_{1.5}\left[1-\left(\tfrac{\nu}{F}\right)^{-5/3}\right]+\dots\ . \end{aligned}$$

Here, the parameters $\tau_0, \tau_1, \dots$ are numerical constants, whose values may be computed from the models.

It is important to notice that in any case (Newtonian or post Newtonian), the signal is a *locally monochromatic* one, in the sense that time and local frequency are in one-to-one correspondence.

For the sake of simplicity, we shall restrict ourselves to the case of the Newtonian approximation. Nevertheless, we shall describe algorithms which may easily be modified to account for post-Newtonian corrections if necessary, at the cost of an increased algorithmic complexity.

The Fourier transform (we shall follow the convention $\hat h(k) = \int h(x)\exp\{-ikx\}dx$) of the signal in (2) may be evaluated via the stationary phase approximation, which yields

$$\begin{aligned} \hat h(k) \ \approx \ &\frac{A}{\sqrt{2\pi\beta F}}\left(\tfrac{k}{2\pi F}\right)^{(2\alpha-\beta+1)/(2\beta)}e^{i\Phi} \\ &\exp\left\{i\left(\tfrac{\beta k}{\beta+1}\left(\tfrac{k}{2\pi F}\right)^{1/\beta}-kx_0+\tfrac{\pi}{4}\right)\right\} \end{aligned} \tag{11}$$

for $k \geq 0$, and $\hat h(-k) = \overline{\hat h}(k)$. Let us stress that this expression should be regarded as a formal approximation (since $h(x)$ in (2) is neither in $L^2(\mathbb{R})$ nor in $L^1(\mathbb{R})$); nevertheless it may considered as a good approximation in a limited frequency range. Such an approximation has been a building block of the matched filter approaches.

It is also interesting to notice that the stationary phase approximation for the Fourier transform has the following invertibility property. If one uses the stationary phase approximation to estimate the inverse Fourier transform of (11), one gets back to the expression in (2), without any correction. Such a property, which we shall use later on, is not particular to this category of signals, and is shared with the locally monochromatic signals. See [28] for a more complete discussion of this point.

B. Noise Model

The expected signal is buried into detector noise, which is the superposition of several contributions, among which the most important are: seismic noise, photon counting noise (shot noise) and thermal noises [1,8,26]. The main contributions to thermal noise are: pendulum thermal noise, mirror thermal noise and wires thermal noise. We shall assume that the seismic noise is deeply reduced above a few Hz by seismic isolation and therefore shall not take it into account in our model. We shall work with simplified noise models, i.e. weakly stationary processes, in which we shall assume that

1. All sources of noise have Gaussian statistics (which is not strictly the case, as was discussed by several authors).
2. The different contributions are uncorrelated.

Thus, using the Cramér representation (see section III D below, and more particularly Eqs (38-40) for more details), we shall write

$$n(x) = \frac{1}{2\pi}\int e^{ikx}\sqrt{\mathcal{E}(k)}dW_k \ , \tag{12}$$

where dW_k is a white noise measure, and $\mathcal{E}(k) = S(k/2\pi)$ is the (two-sided) *power spectral density*, given as follows (the numerical constants are taken from [7]:

$$S(\nu) = S_1\nu^{-5} + S_2\nu^{-1} + S_3\left(1+\left(\frac{\nu}{500Hz}\right)^2\right) + S_v(\nu) \tag{13}$$

where the frequency ν is expressed in Hz. The numerical values, taken from [7], read

- $S_1 = .65\ 10^{-36}Hz^4$ for the pendulum thermal noise.
- $S_2 = .7\ 10^{-42}$ for the mirrors thermal noise.
- $S_3 = 1.45\ 10^{-46}Hz^{-1}$ for the shot noise.

$S_v(\nu)$ accounts for the violin thermal noise, and is given by

$$S_v(\nu) = \sum_{n=1}^{\infty} S_v^{(n)}(\nu) \ , \tag{14}$$

where

$$S_v^{(n)}(\nu) = \frac{1}{\nu}\frac{K}{(\nu^2-\nu_n^2)^2+\phi^2\nu_n^4} \tag{15}$$

for some constant K. The resonant frequencies $\nu_n = n\nu_1$ are multiple of a fundamental frequency ν_1, set to $\nu_1 \approx 250\ Hz$ in our simulations.

In practice, the violin resonances are sharply peaked enough so that at a given frequency, one only has to take into account the contribution of the nearest mode. This implies that for $\nu \approx \nu_n$, we may approximate

$$S_v(\nu) \approx \frac{1}{n^4}\frac{\nu_1}{\nu}\frac{C\phi^2}{\left(\frac{1}{n^2}\frac{\nu^2}{\nu_1^2}-1\right)^2+\phi^2} \ .$$

The choice of the constants C and ϕ^2 (which controls the bandwidth of the resonances) is a tricky problem, since these depend upon mechanical considerations (mirror masses, quality factors of wires,... [7,26]). We have tentatively chosen the conservative values $C \approx S_v(\nu_1) = 1.5\ 10^{-39}\ Hz^{-1}$, and $\phi^2 = 10^{-7}$. Changing these values does not seem to modify the performances of the algorithm described below, at least as long as the average slope of the spectral density in the range $50Hz - 1000Hz$ (i.e. $S(\nu) \sim \nu^{-1}$) is not affected.

The spectral density used in our simulations is displayed in Figure 2, and the numerical values are summarized in Table I.

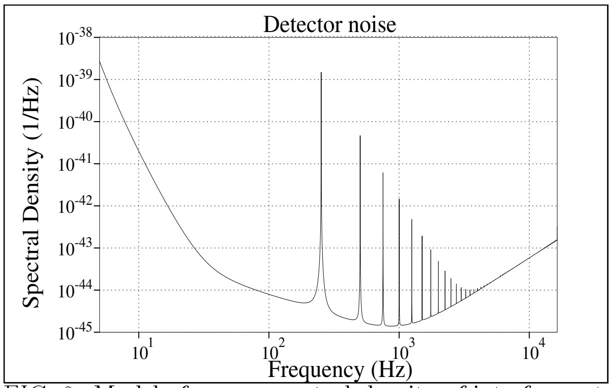

FIG. 2. Model of power spectral density of interferometric detector noise used in the simulations.

III. WAVELET TRANSFORMS

The algorithm we shall describe is essentially based on the continuous wavelet transform and progressive wavelets. We now sketch the main aspects of continuous wavelet analysis [24,25] (see also [15,41]) in the context we are interested in.

A. The Continuous Wavelet Transform

Let us start with some generalities on the continuous wavelet transform, in the version we shall use throughout this paper. Let $\psi(x)$ be an integrable and square-integrable function, such that $\hat{\psi}(k) = 0\ \forall k \leq 0$ and that

$$0 < c_\psi := \int_0^\infty |\hat{\psi}(k)|^2 \frac{dk}{k} < \infty \tag{16}$$

Functions satisfying the above properties are called *progressive wavelets*. Such wavelets may be used to provide alternative representations of signals as follows. Let $f(x)$ be a square-integrable real-valued function, and let $Z_f(x)$ be its analytic signal, defined in the Fourier domain as $\hat{Z}_f(k) = 2\hat{f}(k)\Theta(k)$, $\Theta(k)$ being the Heaviside step function. Then one may write

$$Z_f(x) = \frac{1}{c_\psi}\int T_f(b,a)\psi_{(b,a)}(x)\frac{da\,db}{a^2} \tag{17}$$

where the functions $\psi_{(b,a)}(x)$ are the wavelets, shifted and scaled copies of $\psi(x)$

$$\psi_{(b,a)}(x) = \frac{1}{\sqrt{a}}\psi\left(\frac{x-b}{a}\right) \ , \tag{18}$$

and the coefficients $T_f(b,a)$ defined by

$$T_f(b,a) = \langle f, \psi_{(b,a)}\rangle = \frac{1}{\sqrt{a}}\int f(x)\overline{\psi}\left(\frac{x-b}{a}\right)dx \tag{19}$$

form the *Continuous wavelet transform* of $f(x)$. Obviously, $f(x)$ may be recovered from its analytic signal as $f(x) = \Re Z_f(x)$, where $\Re$ denotes the real part, so that Equation (17) provides a complete analysis-reconstruction scheme.

B. Translation and Scaling Invariance Properties of the wavelet transform.

The continuous wavelet transform enjoys built-in invariance properties. For example, the transform of a shifted copy $f(x-x_0)$ of the signal $f(x)$ equals the corresponding time-shifted copy $T_f(b-x_0,a)$ of the transform $T_f(b,a)$ of $f(x)$. A similar property holds with dilations. More generally if we set

$$\tilde{f}(x) = \frac{1}{\sqrt{\lambda}}f\left(\frac{x-x_0}{\lambda}\right) \ .$$

Then we have

$$T_{\tilde{f}}(b,a) = T_f\left(\frac{b-x_0}{\lambda}, \frac{a}{\lambda}\right) \ . \tag{20}$$

Such properties have found a lot of applications, for example for the study of fractal and multifractal functions and measures.

Let us now show why they have their importance in gravity waves detection problems as well. Let us forget for a while about the constant phase Φ. The signal appearing in Eq. (2) (or more precisely its analytic signal, see Eq. (51) below) is in fact (up to a normalization factor) a shifted and scaled copy of a reference signal

$$f_{\alpha,\beta}(x) = \Theta(-x)x^{\alpha}\exp\left\{ix^{\beta+1}\right\} \ . \tag{21}$$

Therefore, it follows from the invariance properties of the wavelet transform described above, that the transforms of the corresponding signals are obtained from the transform of (21) by translation and dilation. More precisely, we have that

$$Z_f(x) = AF^{-\alpha/(\beta+1)}e^{i\Phi}f_{\alpha,\beta}\left(F^{1/(\beta+1)}(x_0-x)\right) \tag{22}$$

and then

$$\begin{aligned} T_f(b,a) &= AF^{(1-2\alpha)/(2\beta+2)}e^{i\Phi} \\ & \quad T_{f_{\alpha,\beta}}\left(F^{1/(\beta+1)}(x_0-b), F^{1/(\beta+1)}a\right) , \end{aligned} \tag{23}$$

and the detection problem may be reformulated as a detection problem in the time-scale plane: find a translation parameter x_0 and a scale parameter $a_0 = F^{1/(\beta+1)}$ such that $T_f(b,a)$ is a shifted and scaled copy of $T_{f_{\alpha,\beta}}(-b,a)$.

C. Wavelet Transform of Frequency Modulated Signals

We essentially follow here refs [17,38]. Let us consider a model signal of the form

$$f(x) = A(x)\cos\phi(x) \ , \tag{24}$$

where the amplitude and phase functions are assumed to be twice and four times continuously differentiable respectively, and assume that the amplitude $A(x)$ is slowly varying compared to the oscillations. Let us consider a complex-valued (progressive) analyzing wavelet, which we write in the form

$$\psi(x) = A_{\psi}(x)e^{i\phi_{\psi}(x)} \ , \tag{25}$$

and assume for the sake of simplicity that the amplitude $A_{\psi}(x)$ is smooth and maximal at $x=0$, with

$$|\psi(0)| = 1$$

and that the wavelet is a linear phase one, i.e. is such that

$$\phi'_{\psi}(x) = \omega_0 = 2\pi$$

(see [17] for the general case). Then writing the continuous wavelet transform as an oscillatory integral, and approximating the integral by means of the stationary phase method, we obtain the following approximate expression for the wavelet transform of the signal in (24):

$$T_f(b,a) \approx \sqrt{\frac{\pi}{2}}\frac{e^{i\frac{\pi}{4}\mathrm{sgn}(\Phi''_{(b,a)}(x_s))}}{\sqrt{a|\Phi''_{(b,a)}(x_s)|}}\ \overline{\psi}\left(\frac{x_s-b}{a}\right)Z_f(x_s) \ , \tag{26}$$

where $\Phi_{(b,a)}(x)$ is the argument of the integrand, and the symbol $\mathrm{sgn}(x)$ stands for the sign of x

$$\Phi_{(b,a)}(x) = \phi(x) - \phi_{\psi}\left(\frac{x-b}{a}\right) \ , \tag{27}$$

and $x_s = x_s(b,a)$ is a stationary point of the integrand, i.e. a value of the argument such that

$$\Phi'_{(b,a)}(x_s) = 0 \ . \tag{28}$$

In addition, it is assumed that for any (b,a) under consideration, there exists only one such point, and that $\Phi''_{(b,a)}(x_s) \neq 0$ (if not, higher order approximations have to be used).

Such stationary points have a very simple intuitive meaning: they represent the values of the integrand for which the oscillations of the wavelet match perfectly those of the signal.

The approximate wavelet transform in (26) is interesting in many respects. Let us simply point out that it naturally leads to the introduction of the following set of points

$$\{(b,a) \text{ such that } x_s(b,a) = b\} \ , \tag{29}$$

termed the *ridge of the wavelet transform.* Indeed, if we forget for the sake of simplicity about the denominator in (26), we can see that $|T_f(b,a)|^2$ is locally maximum in the neighborhood of the ridge (this follows from the assumptions on the localization of the wavelet). In addition, it is readily verified that the ridge takes the form of a curve in the time-scale plane

$$a = a_r(b) = \frac{\phi'_{\psi}(0)}{\phi'(b)} \ . \tag{30}$$

If the signal is locally monochromatic (see the discussion above), the function $a_r(b)$ is monotonic and we may represent the ridge using the reciprocal function

$$b = b_r(a) = \phi'^{-1}\left(\frac{\phi'_{\psi}(0)}{a}\right) \ . \tag{31}$$

We shall be dealing with the so-called *skeleton of the wavelet transform*, i.e. the restriction of the wavelet transform to its ridge.

$$\mathcal{S}_f(b) = T_f(b, a_r(b)) \ . \tag{32}$$

As shown in [17], the skeleton carries all the information about the signal. To be more specific, let us notice that with our assumptions on the wavelet $\psi(x)$ we have

$$\Phi''_{(b,a)}(x) = -\omega_0\,\frac{a'_r(x)}{a_r(x)^2} \ ,$$

and it follows from Eq. (26) that

$$\mathcal{S}_f(b) = \sqrt{\frac{\pi}{2\omega_0}}\sqrt{\left|\frac{a_r(b)}{a_r'(b)}\right|}\, e^{-i\frac{\pi}{4}\mathrm{sgn}(a_r'(b))}\,\overline{\psi(0)}\; Z_f(b) \quad (33)$$

Hence, assuming that the analyzed function $f(x) \in L^2(\mathbb{R})$, we have

$$\begin{aligned}\int |T_f\ \ (b_r(a),a)|^2 \frac{da}{a} &= \int \left|\frac{a_r'(b)}{a_r(b)}\right| \ |\mathcal{S}_f(b)|^2\, db \\ &= \frac{\pi}{2\omega_0}|\psi(0)|^2 \int |Z_f(b)|^2\, db \\ &= \frac{1}{2}\,||f||^2\end{aligned} \quad (34)$$

Such a property will be of interest later on.

D. Wavelet Transform of Stationary Processes

Given a probability space $(\Omega, \mathcal{B}, \mathbb{P})$ and an order two stochastic process (i.e. a process $n(x) = n_\omega(x)$ such that for all x, $n(x)$ is square integrable with respect to the measure $\mathbb{P}$) with covariance operator C, it is easy to see that if $\mathbb{E}$ denotes the expectation value,

$$\mathbb{E}\{T_n(b,a)\overline{T_n(b',a')}\} = \langle \psi_{(b',a')}, C\psi_{(b,a)}\rangle \ . \quad (35)$$

In the case of weakly stationary processes (assumed to be real valued and of mean zero for the sake of simplicity), the covariance is a convolution operator, so that the autocovariance function

$$\mathcal{C}(\tau) = \mathbb{E}\{n(x+\tau)n(x)\} \quad (36)$$

is a function of the lag τ only. Let $n(x)$ be a weakly stationary stochastic process, and let us assume for the sake of simplicity that it has mean zero. Denote by

$$\mathcal{E}(k) = \int \mathcal{C}(\tau)e^{-ik\tau}d\tau \quad (37)$$

its spectral density. According to the general spectral theory for stationary processes (see e.g. [9,30] for an overview), we shall start with the so-called *Cramér Representation* of $n(x)$

$$n(x) = \frac{1}{2\pi}\int e^{ikx}\sqrt{\mathcal{E}(k)}dW_k \ , \quad (38)$$

where dW_k is a zero mean Gaussian white noise measure, such that

$$\mathbb{E}\{dW_k\} = 0 \qquad \forall k \ , \quad (39)$$

and

$$\mathbb{E}\{dW_k dW_{k'}\} = 2\pi\delta(k-k')dk \ . \quad (40)$$

Thanks to Plancherel's formula and Fubini's lemma, we may use the Cramér representation in (38) to obtain the following representation for the wavelet transform $T_n(b,a)$ of $n(x)$

$$T_n(b,a) = \frac{1}{2\pi}\int e^{ikb}\sqrt{\mathcal{E}(k)}\overline{\hat{\psi}(ak)}dW_k \ , \quad (41)$$

from which we immediately obtain, for all b, a

$$\mathbb{E}\{T_n(b,a)\} = 0 \ , \quad (42)$$

and

$$\mathbb{E}\{|T_n(b,a)|^2\} = \frac{1}{2\pi}\int \mathcal{E}\left(\frac{k}{a}\right)|\hat{\psi}(k)|^2 dk \ . \quad (43)$$

In particular, when $n(x)$ is a white noise, $\mathcal{E}(k) = \sigma^2$ and we get $\mathbb{E}\{|T_n(b,a)|^2\} = \sigma^2||\psi||^2$. The latter property will be useful in what follows.

More generally, we have

$$\begin{aligned}&\mathbb{E}\{T_n(b,a)\overline{T_n(b',a')}\} = \\ &\quad \frac{\sqrt{aa'}}{2\pi}\int e^{ik(b-b')}\overline{\hat{\psi}(ak)}\hat{\psi}(a'k)\mathcal{E}(k)dk\end{aligned} \quad (44)$$

In the case of white noise, we simply get

$$\mathbb{E}\{T_n(b,a)\overline{T_n(b',a')}\} = \sigma^2\,\langle \psi_{(b',a')}, \psi_{(b,a)}\rangle \ . \quad (45)$$

E. A Prewhitening Wavelet Transform

When $\mathcal{E}(k)$ is as in Figure 2, it is easy to see that $\mathbb{E}\{|T_n(b,a)|^2\}$ can vary over several orders of magnitude, which is fairly unconvenient in practice. Such a shortcoming may be avoided as follows.

Let us denote by C the covariance operator associated with the stationary process $n(x)$ described above. C is a convolution operator, which may be written as

$$Cf(x) = \frac{1}{2\pi}\int e^{ikx}\mathcal{E}(k)\hat{f}(k)dk \ . \quad (46)$$

Given such a covariance operator, we define the corresponding *prewhitening wavelet transform* of $f(x) \in L^2(\mathbb{R})$ as follows

$$W_f(b,a) = \langle C^{-1/2}f, \psi_{(b,a)}\rangle = \frac{\sqrt{a}}{2\pi}\int e^{ikb}\frac{\hat{f}(k)\overline{\hat{\psi}(ak)}}{\sqrt{\mathcal{E}(k)}}dk \ . \quad (47)$$

It is easy to check that given a stationary process $n(x)$ of spectral density $\mathcal{E}(k)$, its prewhitening wavelet transform is such that

$$V(a) = \mathbb{E}\{|W_n(b,a)|^2\} = ||\psi||^2 \ . \quad (48)$$

In such cases, if we are given a signal of the form $f(x) = f_0(x) + n(x)$, where $n(x)$ is a weak sense stationary random process with spectral density $\mathcal{E}(k)$, we shall find it convenient to introduce the quantity

$$M(b,a) = |W_f(b,a)|^2 - V(a) \quad (49)$$

Hence, it follows from $\mathbb{E}\{W_n(b,a)\} = 0$, $\forall b, a$ that

$$\mathbb{E}\{M(b,a)\} = |W_{f_0}(b,a)|^2 \ . \quad (50)$$

IV. A DETECTION ALGORITHM

Let us now turn to the purpose of this paper, namely the description of a wavelet based algorithm for the detection of binary coalescences and the corresponding parameter estimation problem. Our main tool will be the prewhitening wavelet transform described above. But for the sake of simplicity let us proceed step by step: we shall start with the description of the algorithm in the non-noisy situation, then describe the case of noisy signals with white noise; we shall then be ready to address the modifications needed to account for more realistic situation.

As we said in the introduction, we shall stick to the case of the Newtonian situation, which might be sufficient for the detection problem (in which case post-Newtonian corrections may be taken care of in the parameter estimation stage of the detection). If $\psi(x)$ is a progressive wavelet with linear phase $\phi_\psi(x) = \omega_0 x$, the continuous wavelet transform of the binary coalescence signal is given as in Eq. (26), where $Z_f(x)$ is the analytic signal of the signal $f(x)$ in (2), approximately given by

$$\begin{aligned} Z_f(x) = \; & A(x_0 - x)^\alpha \Theta(x_0 - x) \\ & \exp\left\{ i \left[\Phi - \tfrac{2\pi}{\beta+1} F (x_0 - x)^{\beta+1} \right] \right\} \; . \end{aligned} \tag{51}$$

Remark: As before, let us stress that such an approximation is only valid in the intermediate frequency range (see the remarks above). We refer to [28] for a more detailed discussion of this point.

The ridge of the wavelet transform is of the form

$$a_r(b) = \frac{\omega_0}{2\pi F}(x_0 - b)^{3/8} \; . \tag{52}$$

Equivalently, we shall also consider the reciprocal function

$$b_r(a) = x_0 - \left(\frac{2\pi a F}{\omega_0} \right)^{8/3} \; , \tag{53}$$

hereafter termed *group delay.* It is in fact more convenient to work with the group delay rather than the local frequency, because of the form of the signal. This will in particular make easier the implementation of post-Newtonian corrections, which are given explicitely in terms of group delay.

Given a candidate (τ, γ) for the pair (x_0, F), we consider the corresponding ridge candidate

$$b_{(\tau,\gamma)}(a) = \tau - \left(\frac{2\pi a \gamma}{\omega_0} \right)^{8/3} \; , \tag{54}$$

and the following *line integral*

$$\mathcal{L}_f(\tau, \gamma) = \int M(b_{(\tau,\gamma)}(a), a) \frac{da}{a} \; . \tag{55}$$

Here, $M(b, a)$ will denote generically a time-scale representation, which we shall choose according to the situation under consideration. Basically, $\mathcal{L}_f(\tau, \gamma)$ is the integral along the ridge candidate of the "energy" of the transform. The choice of this particular form, and more specially of the integration measure, will become clear in the following subsections.

We now describe some particular situations with increasing complexity.

A. The Non-Noisy Case

To understand the behavior of the quantity introduced in (55), let us consider first the "pure case"

$$f(x) = A h_F(x_0 - x) \; ,$$

with $h_F(x)$ defined in (2). Then, if we choose

$$M(b, a) = |T_f(b, a)|^2$$

we can see that

$$\mathcal{L}_f(x_0, F) \approx \frac{\pi}{\phi'_\psi(0)} |\psi(0)|^2 \, ||f||^2 = \frac{A^2}{2} ||h_F||^2$$

(this follows from the stationary phase approximation; the factor 1/2 just comes from the fact that progressive wavelets only see the positive frequency part of the signal-and the noise-) and that $\mathcal{L}_f(\tau, \gamma)$ is (at least approximately) maximal for $(\tau, \gamma) = (x_0, F)$.

This suggests to search the pair (x_0, F) by maximizing the line integral $\mathcal{L}_f(\tau, \gamma)$ with respect to τ and γ simultaneously (the details of the implementation are given in subsection IV D below).

B. The White Noise Case

Let us now consider the situation where the signal is buried into a white noise, denoted by $w(x)$:

$$f(x) = A h_F(x_0 - x) + w(x) \; .$$

In such a case, it is more convenient to work with the following time-scale representation

$$M(b, a) = |T_f(b, a)|^2 - V(a) \; ,$$

where $V(a) = \mathbb{E}\{|T_w(b, a)|^2\}$ may be either computed in advance (in which case we have $V(a) = ||\psi||^2$, see Eq. (48) above), or estimated from the data. In such a case, repeating the considerations of the previous section, we have that

$$\mathbb{E}\{\mathcal{L}_{h_F}(x_0, F)\} \approx \frac{\pi A^2}{\phi'_\psi(0)} |\psi(0)|^2 \, ||h_F||^2 = \frac{A^2}{2} ||h_F||^2$$

and we can proceed as before, i.e. maximize the line integral $\mathcal{L}_f(\tau, \gamma)$ with respect to τ and γ simultaneously.

C. The General Situation

Let us finally consider the realistic situation

$$f(x) = Ah_F(x_0 - x) + n(x) \ , \tag{56}$$

where $h_F(x)$ is given in (2) and $n(x)$ is a weakly stationary stochastic process with spectral density $\mathcal{E}(k)$, modeling the detector noise. In such a case, it is more convenient to use the prewhitening wavelet transform introduced in Section III E. We then choose

$$M(b,a) = |W_f(b,a)|^2 - V(a) \ , \tag{57}$$

where

$$V(a) = \mathbb{E}\{|W_n(b,a)|^2\} \tag{58}$$

represents the "typical contribution of the noise at scale a" (and does not depend on b, as a consequence of the stationarity of the noise), and may be either precomputed or estimated from the data as before.

This procedure introduces an additional difficulty. Indeed, the ridges of $f(x)$ and $C^{-1/2}f(x)$ need not be identical. However, if in the frequency range under consideration the spectral density $\mathcal{E}(k)$ of the noise is a slowly varying function of the frequency k, the two ridges may be considered equal, to a good approximation. This is based on the following argument. The prewhitening is a multiplication of the fourier transform in (11) with $\mathcal{E}(k)^{-1/2}$. If this function is slowly varying enough, then the stationary phase approximation may be used again to estimate the inverse Fourier transform of the product, and yields an approximation of the form

$$C^{-1/2}f(x) \approx \frac{f(x)}{\sqrt{\mathcal{E}(2\pi\nu(x))}} \tag{59}$$

where $\nu(x)$ is the local frequency given in (7). Of course, such an approximation fails for x close to x_0 and as x goes to $-\infty$, but it is worth pointing out that in these two limits, the amplitude of $C^{-1/2}f(x)$ goes to zero. A similar argument may be developed for higher order post-Newtonian approximations.

Thus, the detection algorithm we propose is based on the following maximization problem

$$\max \mathcal{L}_f(\tau,\gamma) = \int M(b_{(\tau,\gamma)}(a), a)\frac{da}{a} \ , \tag{60}$$

with $M(b,a)$ given in (57). Notice that owing to the discussions of the previous two subsections,

$$\mathbb{E}\{\mathcal{L}_f(x_0,F)\} \approx \frac{A^2}{2}||C^{-1/2}h_F||^2 \ . \tag{61}$$

Thus the peak value of the output of the algorithm behaves like that of the matched filter (up to a factor 1/2, due to the fact that we are only dealing with the positive frequency part of the signal and the noise, as we already explained).

D. The Maximization Algorithm

We now explain our implementation of the maximization algorithm (60), in the situation given in Eq. (56), with $h_F(x)$ as in (2) and $\mathcal{E}(k)$ as in (13). In the Newtonian situation, it amounts to a search in a two-dimensional parameter space, parametrized by the pair (x_0, F). The goal was to derive an algorithm compatible with a possible real time implementation.

The first point is to fix a criterion to decide of a possible detection. This is done by fixing a certain threshold, hereafter denoted by `THRESHOLD` for the line integral (55). The choice of this threshold is based upon an a priori knowledge of the noise, and some a priori estimates on the false alarm or non detection probabilities. We shall not go into details on these aspects here.

Based on the discussion above, let us introduce the following notations. for a given date τ, set

$$\hat{F}(\tau) = \arg\max_\gamma \mathcal{L}_f(\tau,\gamma) \ , \tag{62}$$

and

$$\hat{\mathcal{I}}(\tau) = \max_\gamma \mathcal{L}_f(\tau,\gamma) \ , \tag{63}$$

Notice that $\hat{\mathcal{I}}$ is an estimator for $A^2||h_F||^2/2$.

Our approach relies on a two-step optimization, as follows

- `FOR` $\tau = \tau_{min}$ `TO` $\tau = \tau_{max}$
    1. Solve the maximization problem in (63) with respect to γ.
    2. Store the values $\hat{F}(\tau)$ and $\hat{\mathcal{I}}(\tau)$.
- `IF` $\hat{\mathcal{I}}(\tau) \geq$ `THRESHOLD`: mark τ as a possible date for an event, and $\hat{F}(\tau)$ as an estimate for the parameter F.

The maximization is carried out as follows. In order to improve the stability of the method, the domain under consideration for the frequency parameter F (say the range $25\,Hz - -150\,Hz$) is split into several subdomains (5 subdomains in our simulations), and a standard maximization method (an adapted version of Brent's parabolic search method [34,37]) is used within each domain. We then keep the maximal value $\hat{\mathcal{I}}(\tau)$ of the line integral among the maxima in the subdomains, and the corresponding value $\hat{F}(\tau)$ for the frequency parameter F.

V. NUMERICAL RESULTS

We present here some of the numerical results which we obtained with the algorithm we described above. The algorithm was implemented on Unix workstation using the C language. It mainly relies on two steps, which we outline here

1. Prewhitening wavelet transform: the prewhitening wavelet transform (47) of the signal is computed and stored into memory. The expectation value in (48) is estimated, and the predenoised transform (49) is computed.

2. The minimization problem in Eq. (63) is solved for all candidates x_0, yielding estimators for the amplitude and the frequency.

In practice, since the spectral density may vary slowly as a function of time, it may be desirable to include into the algorithm a spectral estimation procedure before steps 1 and 2:

- Spectral estimation: the spectral density of the detector noise is estimated from the signal itself, or from a "pure noise" reference if there is such a reference available.

The numerical tests have been performed on signals generated following the lines of Section II. We have followed steps 1 and 2 above, without the spectral estimation step (the spectral density is assumed to be known).

A. Some examples

We now present some examples of simulated detections achieved by the algorithm described above. We have used the so-called Morlet's wavelet

$$\psi(x) = e^{-x^2/2} e^{i\omega_0 x} \tag{64}$$

with $\omega_0 = 2\pi$, and computed the wavelet transform on a lattice of the form (b_k, a_j) with $b_k = k\nu_s$ and $a_j = 2a_0^j$, with $a_0 = 2^{1/8}$ and $j = 0, \dots 39$.

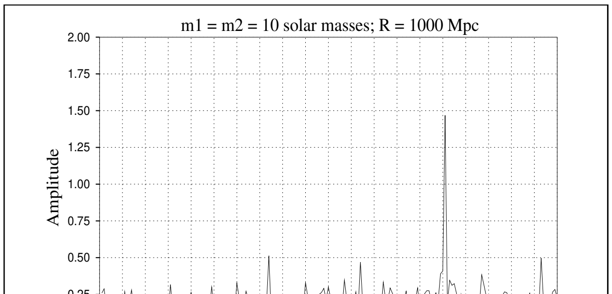

FIG. 3. Output $\hat{\mathcal{I}}(\tau)$ of the detection algorithm for a gravitational wave generated by a coalescing system of masses $m_1 = m_2 = 10M_\odot$, at a distance $R = 1Gpc$. Sampling frequency: $\nu_s = 1000Hz$.

As a first illustration, we display in Figure 3 the output of the algorithm, i.e. the function $\mathcal{I}(\tau)$ defined in Eq (63), for the case of a system formed of two neutron stars of 10 solar masses each, at a distance of 1 Gpc. The sampling frequency was set to $\nu_s = 1000\,Hz$. The event was suposed to take place at $x_0 = 15.1sec$. A significant peak is clearly seen, at the correct location (see subsection V B below for more details on statistical aspects and significance levels). The estimated value $\hat{F}$ for the F parameter was $\hat{F} = 39.5$ instead of $F = 39.05$, and the maximal amplitude was $\hat{\mathcal{I}} = 1.468$.

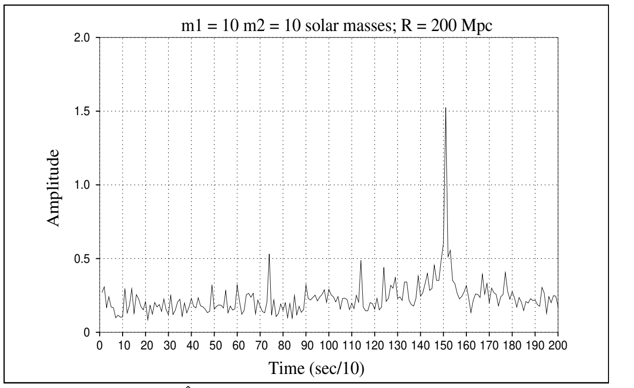

FIG. 4. Output $\hat{\mathcal{I}}(\tau)$ of the detection algorithm for a gravitational wave generated by a coalescing system of masses $m_1 = 10M_\odot$, $m_2 = 1M_\odot$, at a distance $R = 200Mpc$. Sampling frequency: $\nu_s = 1000Hz$.

As another example, we display in Figure 4 the function $\hat{\mathcal{I}}(\tau)$ in the case of a system formed of two neutron stars of 10 and 1 solar masses respectively, at a distance $R = 200\,Mpc$. The sampling frequency was set to $\nu_s = 1000\,Hz$. Notice again a significant peak at the correct location. The estimated value $\hat{F}$ for the F parameter was $\hat{F} = 84.1$ instead of $F = 85.97$, and the maximal amplitude was $\hat{\mathcal{I}} = 1.525$.

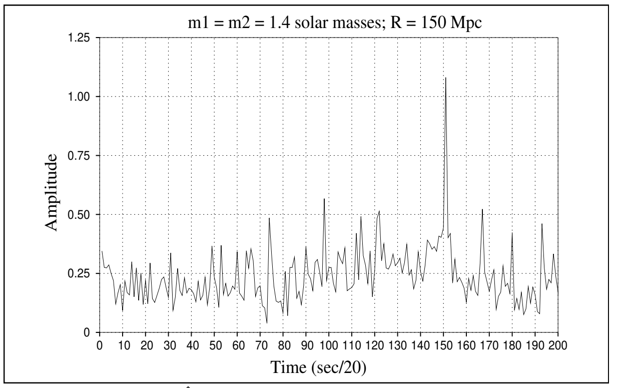

FIG. 5. Output $\hat{\mathcal{I}}(\tau)$ of the detection algorithm for a gravitational wave generated by a coalescing system of masses $m_1 = m_2 = 1.4M_\odot$, at a distance $R = 150Mpc$. Sampling frequency: $\nu_s = 2000Hz$.

Finally, we show in Figure 5 the function $\hat{\mathcal{I}}(\tau)$ in the case of a system formed of two neutron stars of 1.4 solar masses each, coalescing at a distance of $R = 150Mpc$. Since the signal presented higher frequencies than the previous ones, we found convenient to increase the sampling frequency and thus set it to $\nu_s = 2000Hz$. Again the event is correctly detected. The estimated value was $\hat{F} = 134.67$, whereas the correct one is $F = 133.47$, and the peak value was $\hat{\mathcal{I}} = 1.08$. Again, we postpone the discussion of significance to the next subsection.

B. Simulations and parameter estimations

We describe in this section the results of simulations. The goal of the first simulations is to study the statistics of the functions $\hat{\mathcal{I}}(\tau)$ and $\hat{F}(\tau)$ and estimate critical values for $\hat{\mathcal{I}}$ in order to set up significance levels for detection criteria. We ran simulation algorithm in a "noise alone" situation, for three different values of the sampling frequency.

We show in Figures 6 and 7 the histograms of the amplitudes $\hat{\mathcal{I}}(\tau)$ in the "noise alone" case, for a sampling frequency set to $\nu_s = 1000Hz$ and $\nu_s = 2000Hz$ respectively. The values of the sample means μ, standard deviations σ, medians m, as well as the 1%, 0.5% and 0.1% critical values $z_{0.01}$, $z_{0.005}$ and $z_{0.001}$ are listed in Table II (with z_q defined by $\mathbb{P}\{\hat{\mathcal{I}} \geq z_q\} = q$). The histograms and these values are seen to depend weakly on the sampling frequency.

Coming back to the examples of subsection V A we remark that the critical values in Table II clearly indicate that the peaks obtained in the simulations described above are definitely significant, since the value of $\hat{\mathcal{I}}$ is much larger than $z_{0.001}$.

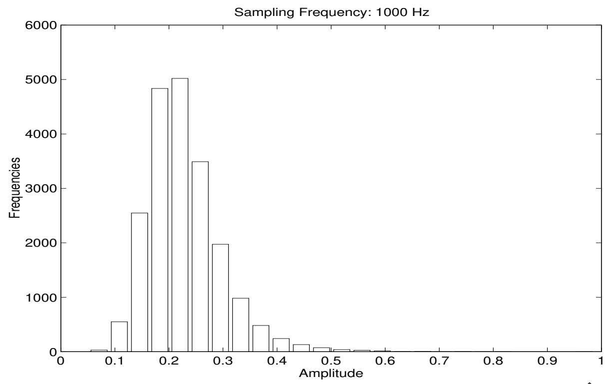

FIG. 6. Histogram of the distribution of amplitudes $\hat{\mathcal{I}}$, in a "noise alone" situation; 20000 realizations, grouped into 25 classes. Sampling frequency: $\nu_s = 1000Hz$.

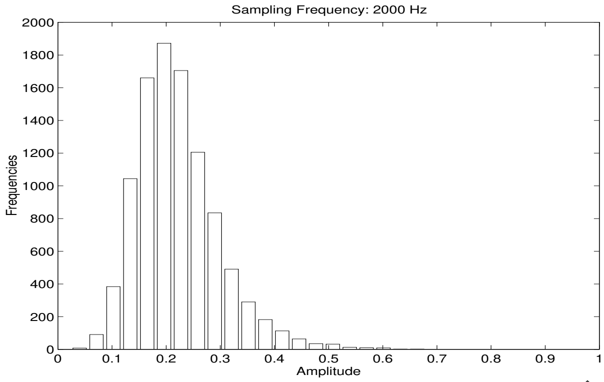

FIG. 7. Histogram of the distribution of amplitudes $\hat{\mathcal{I}}$, in a "noise alone" situation; 10000 realizations, grouped into 25 classes. Sampling frequency: $\nu_s = 2000Hz$.

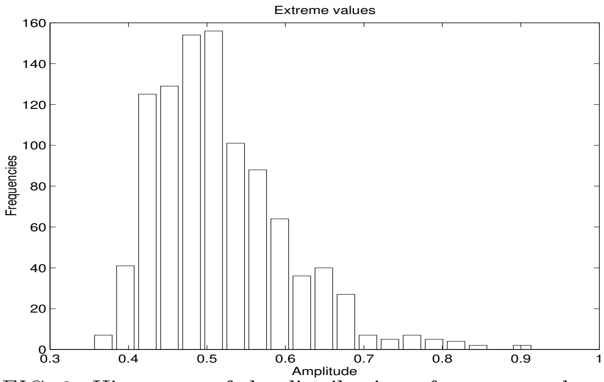

FIG. 8. Histogram of the distribution of extreme values of the algorithm, in a "noise alone" situation; 1000 realizations, grouped into 25 classes. Sampling frequency: $\nu_s = 1000Hz$.

The distribution of extreme values is also of interest. In the same conditions as before, we generated a series of $N = 1000$ realizations of stationary noise with spectral density given in (13), on which we ran the detection algorithm. The sampling frequency was set to $\nu_s = 1000Hz$, and the duration of each signal was $65sec$. For each realization i, the function $\hat{\mathcal{I}}(\tau)$ was evaluated, and the maximum $\hat{\mathcal{I}}_i$ of $\hat{\mathcal{I}}(\tau)$ was stored. We give in Figure 8 the histogram of these values (min = 0.354, max = 0.916). The mean, median, standard deviation and critical values of the distribution of extreme values are given at the bottom of Table II.

To evaluate the performances of the detection algorithm, we considered the three situations shown in subsection V A. Namely, the cases of binary systems of masses $m_1 = m_2 = 10M_\odot$, $m_1 = 1M_\odot$, $m_2 = 10M_\odot$, and $m_1 = m_2 = 1.4M_\odot$ solar masses, at distances $R = 1\,Gpc$, $R = 200\,Mpc$ and $R = 150\,Mpc$ respectively. We generated 1000 realizations of each of these situations. We ran the detection algorithm on each of them, and collected the corresponding values for the coalescence time $\hat{x}_0$, the frequency parameter $\hat{F}$ and the amplitude parameter $\hat{\mathcal{I}}$.

As an example, we show in Figure 9 the histogram of the amplitudes $\hat{\mathcal{I}}$ for the case $m_1 = m_2 = 1.4M_\odot$,

$R = 150Mpc$. All the values of $\hat{\mathcal{I}}$ are larger than the critical value $z_{0.001}$. A more careful analysis of the results indicates that out of 1000 realizations (corresponding to approximately 3 hours of signal), the detection was not correct on four of them, in the sense that either the date $\hat{x}_0$ or the frequency $\hat{F}$ was far away from the expected value.

As a by-product, the detection algorithm also gives an estimator for the frequency parameter F (and therefore the chirp mass $\mathcal{M}$, via Eq. (4)). We display in Figure 10 the histogram of estimated frequencies $\hat{F}$. The histogram is peaked near the correct value, namely $F \approx 133$.

A similar analysis was performed in the two other situations, in which the algorithm didn't produce any incorrect detection or estimation. The results are summarized in Tables III and IV , where the values of $\hat{F}$ are compared with the expected values F.

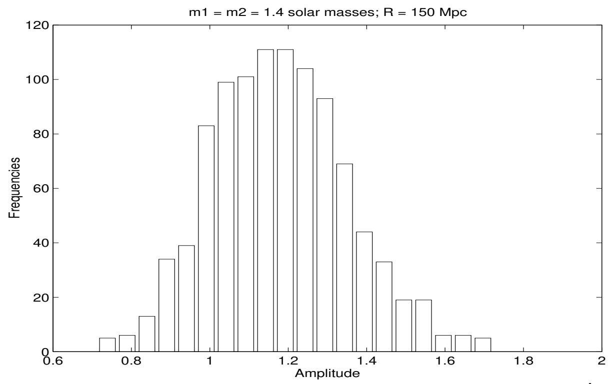

FIG. 9. Histogram of the distribution of amplitudes $\hat{\mathcal{I}}$, in the case $m_1 = m_2 = 1.4M_\odot$, $R = 150$; 1000 samples, grouped into 20 classes. Sampling frequency: $\nu_s = 2000Hz$.

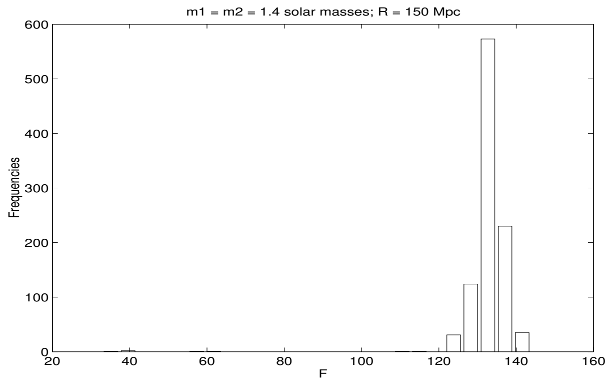

FIG. 10. Histogram of the distribution of frequencies $\hat{F}$, in the case $m_1 = m_2 = 1.4M_\odot$, $R = 150Mpc$; 1000 samples, grouped into 25 classes. Sampling frequency: $\nu_s = 2000Hz$.

VI. CONCLUSIONS

We have presented in this paper a new method for on line processing of interferometric detector signals and binary coalescence detection. The approach is based on an adapted version of the continuous wavelet transform, coupled with a suitable optimization algorithm, and is very much in the spirit of previous works by the authors [10,12,17,29].

Our method bears some similarities with some algorithms already published in the literature [21,42], and [19] before. However, ours implements significant improvements such as the introduction of the prewhitening wavelet transform described in Section III E, the optimization of an energy function $\mathcal{L}_f(\tau,\gamma)$ in Eq. (60) based on a one-dimensional integral instead of a two-dimensional one, and the use of a maximization method for the optimization, instead of a blind search. In addition, estimates such as (61), which makes the connection with matched filter methods, were not available in the above mentioned approaches.

It is our goal to propose an algorithm, whose performances approach those of traditional matched filter methods, and would be more efficient from computational point of view. We have shown that our algorithm is able to detect coalescence events (with reasonable values of the mass parameters) at distances up to $150Mpc$ (in the case of optimal orientation). Such performances, eventhough not as good as what is expected from traditional matched filter techniques, are nevertheless comparable. On the other hand, let us stress that even without any optimization effort in the implementation, our detection algorithm works in real time in a “standard” Unix workstation (it takes approximately 20 seconds to process 40 seconds of signal). In addition, wavelet transforms may be easily implemented in a very efficient way, thanks to the existence of fast algorithms [15,44] (hardware implementations are possible as well).

All together, we believe that the approach presented in this paper should be considered as a serious candidate for on line detection of binary coalescence.

Our analysis was limited to the treatment of signals given in a Newtonian approximation. The extension to higher order post-Newtonian approximations may go into two main directions:

1. Analyze the performances of the current algorithm on restricted post-Newtonian signals, and evaluate the loss in output signal to noise ratio created by the mismatch.

2. Modify the present algorithm in order to accomodate post-Newtonian corrections. Such a modification is fairly easy to implement, since it only involves for each τ an optimization in higher dimensional spaces (i.e. the space of parameters $\tau_0, \tau_1, \tau_{1.5}\ldots$), but at the price of an increase of the computational cost.

These aspects, as well as some additional statistical issues, will be addressed in a forthcoming publication.

Acknowledgements: The first author is also with ESM2, IMT-Technopole de Chateau-Gombert, 13451

Marseille, Cedex 20, FRANCE, and the VIRGO group, Orsay.

We wish to thank R. Carmona, A. Grossmann, Ph. Tchamitchian, J.Y. Vinet and W.L. Hwang for stimulating discussions, and A. Królak for inviting us to the Banach semester on *Mathematical Aspects of Gravitation* where we benefited from many advices from experts.

This paper was written after the ultimely departure of our friend and collaborator Bernard Escudié. Bernard has been one of the pioneers of time-frequency signal processing. This work owes a lot to his ideas.

---

[1] A. Abramovici et al. (1992): LIGO: the Laser Interferometer Gravitational-Wave Observatory, *Science*, 256, p. 325-333.

[2] A. Antoniadis & G. Oppenheim Eds (1994): proceedings of the conference *Wavelets and Statistics*, Villard de Lans, France, Lecture Notes in Statistics.

[3] F. Auger and P. Flandrin (1993): Improving the Readability of Time-Frequency and Time-Scale Representations by the Reassignment Method, Technical Report 93.05, Laboratoire d'automatique, Ecole Centrale de Nantes.

[4] R. Balasubramanian, B.S. Sathyaprakash and S.V. Dhurhandar (1995): Gravitational Waves from Coalescing Binaries: Detection Strategies and Monte Carlo Estimation of Parameters, *Phys. Rev.* D 53, vol. 6 pp. 3033-3055.

[5] L. Blanchet, T. Damour and B.R. Iyer (1995): Phys. Rev. D 51, p. 5360.

[6] B. Boashash (1992): Estimating and Interpreting the Instantaneous Frequency of a Signal, Part I: Fundamentals. *Proc. IEEE* **80**, pp. 520–538; Part II: Applications and Algorithms. *Proc. IEEE* **80**, pp. 540–568.

[7] F. Bondu (1996): *Etude du bruit thermique et stabilisation en fréquence du laser du détecteur interférométrique d'ondes gravitationnelles VIRGO.*

[8] C. Bradaschia et al. (1990): *Nucl. Instrum. Methods Phys. Res.* A 518.

[9] D.R. Brillinger, *Time Series; Data Analysis and Theory*, Holden Day Inc. (1981).

[10] R. Carmona, W.L. Hwang, B. Torrésani (1995): *Characterization of signals by the ridges of their wavelet transform*, IEEE Trans. Signal Processing, submitted.

[11] R. Carmona, W.L. Hwang, B. Torrésani (1995): *Multiridge Detection and Time-Frequency Reconstruction*, IEEE Trans. Signal Processing, submitted.

[12] R. Carmona, W.L. Hwang, B. Torrésani (1996): *Practical Time-Frequency Analysis*, Monograph, to be published.

[13] J.M. Combes, A. Grossmann, Ph. Tchamitchian Eds. (1989): *Wavelets, Time-Frequency Methods and Phase Space*, IPTI, Springer Verlag.

[14] K. Danzmann et al. (1994): GEO600, Proposal for a 600 m Laser-Interferometric Gravitational Wave Antenna.

[15] I. Daubechies (1992): Ten Lectures on Wavelets. *CBMS-NFS Regional Series in Applied Mathematics* 61.

[16] M.H.A. Davis (1989): A review of the statistical theory of signal detection in *Gravitational Wave Data Analysis*, B.F.Schutz Ed., Kluwer Academic Publishers.

[17] N. Delprat, B. Escudié, P. Guillemain, R. Kronland-Martinet, Ph. Tchamitchian, B. Torrésani (1992): Asymptotic wavelet and Gabor analysis: extraction of instantaneous frequencies. *IEEE Trans. Inf. Th.* **38**, pp. 644-664.

[18] R.B. Dingle (1973): *Asymptotic expansions, their derivation and interpretation*, Academic Press.

[19] B. Escudié, B. Torrésani (1990): Wavelet representation, time-scaled matched receiver for asymptotic sonar signals emitted by bats. Proceedings of the EUSIPCO conference, Barcelona, *Signal Processing* **V**, vol.1, pp. 305-308.

[20] L.S. Finn and D. F. Chernoff (1993): Observing Binary Inspiral in Gravitational Radiation: one interferometer, *Phys. rev.* **D 47**, vol. 6, pp. 2198-2219.

[21] R. Flaminio, L. Massonnet, B. Mours, S. Tissot, D. Verkindt and M. Yvert(1994): Fast Trigger Algorithms for Binary Coalescences, *Astroparticle Physics* 2, pp. 235-248.

[22] P. Flandrin (1993): Temps-Fréquence. *Traité des Nouvelles Technologies, série Traitement du Signal, Hermes.*

[23] D. Gabor (1946): *Theory of communication*, J. Inst. Elec. Eng. 903, p. 429.

[24] A. Grossmann, R. Kronland-Martinet, J. Morlet (1989): *Reading and understanding the continuous wavelet transform*, in [13].

[25] A. Grossmann, J. Morlet (1984): *Decomposition of Hardy functions into square integrable wavelets of constant shape*, SIAM J. of Math. An. 15,723.

[26] P. Hello (1993): *Ondes Gravitationnelles: Méthodes de Détection.* Ecole d'été de Physique des Particules, Gif sur Yvette.

[27] J.M. Innocent (1994): *Remarks about the Detection of Coalescent Binaries*, VIRGO technical report.

[28] J.M. Innocent and B. Torrésani (1996): *Wavelet Transform and Binary Coalescence Detection*, Preprint CPT-96/P.3363, to appear in the Banach Center Publications, *Mathematical Aspects of Gravitation.*

[29] J.M. Innocent, J.Y. Vinet (1992): *Time-Frequency Analysis of Gravitational Signals from Coalescing Binaries*, VIRGO technical Report.

[30] L.H. Koopmans (1995): *The spectral Analysis of Time Series.* Probability and Mathematical Statistics 22, Academic Press.

[31] A. Królak, P. Trzaskoma (1996): Application of the Wavelet Analysis to Estimation of Parameter of the Gravitational-Wave Signal from a Coalescing Binary, *Classical and Quantum Gravity* 13, pp. 813-830.

[32] S. Mallat (1989): Multiresolution Approximation and Wavelets, *Trans. AMS* 615, 69-88.

[33] Y. Meyer, *Ondelettes et opérateurs* (1989), Hermann.

[34] W.H. Press, S.A. Teukolsky, W.T. Vetterling and B.P. Flannery (1992): *Numerical Recipes: the Art of Scientific Computing*, Second Edition, Cambridge University Press.

[35] B. Picinbono and W. Martin (1983): Représentation des signaux par amplitude et phase instantanées.*Annales des*

Télécommunications **38** , pp. 179-190.
[36] S. Smith (1987): Phys. Rev. D36, p. 2901.
[37] J. Stoer and R. Bulirsch (1991): *Introduction to Numerical Analysis*, Texts in Applied Mathematics 12, Springer Verlag.
[38] Ph. Tchamitchian, B. Torrésani (1991): *Ridge and Skeleton extraction from wavelet transform*, in *Wavelets and their Applications*, M.B. Ruskai & Al Eds, Jones&Bartlett, Boston.
[39] K.S.Thorne (1987): Gravitational Radiation, in *300 Years of Gravitation*, Hawking & Israel Eds, Cambridge University Press.
[40] K.S. Thorne (1996): Gravitational Waves from Compact Objects, proceedings of the IAU Symposium 165, J. van Paradijs, E. van der Heuvel and E. Kuulkers Eds, Kluwer.
[41] B. Torrésani (1995): *Analyse Continue par Ondelettes*, Coll. Savoirs Actuels, InterEditions/Editions du CNRS (in French; English version to appear at SIAM).
[42] D. Verkindt (1993): *Etude d'algorithmes rapides de recherche d'un signal d'onde gravitationnelle provenant de coalescence d'étoiles binaires*, PhD Thesis, Université de Savoie (in French).
[43] J. Ville (1948): Théorie et Applications, de la Notion de Signal Analytique, *Cables et Transmissions* **2** 61-74.
[44] M.V. Wickerhauser (1994): Adapted Wavelet Analysis, from Theory to Software. *A.K. Peters Publ.*

TABLE I. Numerical values of constants in the simulation of the noise.

S_1	S_2	S_3	C	ϕ^2
$.65\ 10^{-36}$	$.7\ 10^{-42}$	$1.45\ 10^{-46}$	$1.5\ 10^{-39}$	$1.\ 10^{-7}$

TABLE II. Top: critical values of the distribution of $\hat{\mathcal{I}}$ in the "noise alone" case for $\nu_s = 1000, 2000$ and $3000Hz$. Bottom: critical values of the distribution of extreme values of $\hat{\mathcal{I}}$ in the "noise alone" case for $\nu_s = 1000Hz$.

ν_s	$\langle\hat{\mathcal{I}}\rangle$	$\sigma_{\hat{\mathcal{I}}}$	$m_{\hat{\mathcal{I}}}$	$z_{0.01}$	$z_{0.005}$	$z_{0.001}$
1000	.228	.069	.218	.449	.495	.594
2000	.222	.077	.211	.464	.516	.604
3000	.215	.087	.203	.485	.532	.656
1000	.517	.0.08	.502	.783	.824	-

TABLE III. Characteristics of the distribution of $\hat{\mathcal{I}}$ for three different masses and distance configurations.

m_1	m_2	$\mathcal{M}$	R	ν_s	$\langle\hat{\mathcal{I}}\rangle$	$\sigma_{\hat{\mathcal{I}}}$	$m_{\hat{\mathcal{I}}}$
1.4	1.4	1.22	150	2000	1.18	0.17	1.17
10	1	2.47	200	1000	1.50	0.21	1.49
10	10	8.70	1000	1000	1.93	0.38	1.92

TABLE IV. Characteristics of the distribution of $\hat{F}$ for three different masses and distance configurations.

m_1	m_2	R	ν_s	F	$\langle\hat{F}\rangle$	$\sigma_{\hat{F}}$	$m_{\hat{F}}$
1.4	1.4	150	2000	133.47	132.91	7.10	133.39
10	1	200	1000	85.97	86.14	2.63	85.84
10	10	1000	1000	39.05	38.49	0.86	38.51